Fully deterministic analysis on photonic whispering-gallery modes of irregular polygonal microcavities with testing in hexagons

Xiaoxuan Luo, Yin Cai, Yongsheng Wang ®, Zaoyu Chen, Fu Liu ®, Lei Zhang ®, Yanpeng Zhang, and Feng Li ®[*]

Key Laboratory for Physical Electronics and Devices of the Ministry of Education & Shaanxi Key Lab of Information Photonic Technique,
School of Electronic Science and Engineering, Faculty of Electronic and Information Engineering,
Xi'an Jiaotong University, Xi'an 710049, China

Polygonal microcavities supporting whispering-gallery modes (WGMs) are widely investigated for optoelectronic applications. Recently, polygonal microcavities with reduced symmetry of various types have been realized in a large number of materials, while the corresponding theoretical analysis of WGMs was either absent or done only for individual cavity shapes. We perform a systematic analysis of irregular polygonal microcavities in general, allowing us to obtain deterministic conclusions on WGMs for all possible parameters of all types of shape irregularities from a set of analytical equations and inequalities. We test the theory with several typical irregular hexagonal microcavities that were experimentally reported, and we discuss the loss mechanism verified by wave optics simulations. The results provide a powerful analyzing tool for experimentalists working on irregular polygonal microcavities, and they constitute a significant extension to the scope of WGM theory.

Whispering-gallery mode (WGM) is one of the most significant mechanisms of light confinement leading to optical microcavities of a very high quality factor (Q-factor). It is found in a wide range of applications, including optical nonlinearity [1–3], frequency combs [4–7], microlasers [3,8–10], sensors [11–15], optical isolators [16], etc. In addition to the regular and deformed circular microcavities such as microdisks, microspheres, and microtoroids that enable a high Q-factor, directional emission, and chaotic-WGM tunneling [17,18], regular polygonal microcavities have been widely investigated for unidirectional microlasers and waveguide-integrated on-chip coherent light sources [19,20], among which the regular hexagonal cavity is most intensively studied, via either top-down [20] or bottom-up grown microstructures and nanostructures [21,22]. It is well known that a regular hexagonal microcavity supports both hexagonal and triangular WGM orbits, the former of which exhibits pseudointegrable leakage. On the other hand, hexagonal cavities with reduced symmetry also emerge in a large variety of optical materials, usually as a natural result of bottom-up grown methods. A large variety of irregular shapes can be produced even within one process of fabrication, especially for those of perovskites [23–28], GaN microdisks [29,30], In_2O_3 microwires [31], ZnO microfences [32], ZnO microwires [33–35], ZnO microcombs [36], organic microcrystals [37–39], and silicon nanopillar quantum wells [40]. Nevertheless, the corresponding theoretical models of WGM were either absent or restricted to the experimentally studied cavity with fixed shape parameters. There remain, therefore, questions regarding what kinds of shape irregularities allow stable WGMs in general, and how the light confinement of

a cavity changes with a continuous variation of the shape parameters. These questions are especially important for N-WGMs with N-sided polygonal photon trajectories (N is the number of polygon sides) that reflect successively on every adjacent side of the polygonal cavity, which in principle enable the maximum reflection angle and thereby the lowest requirement of material refractive index to reach total internal refraction (TIR). To answer such questions, one will require a fully deterministic analysis of geometry for the entire sets of shape variables of all types of irregularities, rather than inductive conclusions drawn from specific sets of shape parameters.

In this Letter, we perform a systematic analysis on WGMs in irregular polygonal cavities by direct analytical solutions of geometry. We first derive the general criterion for the existence of N-WGMs in an N-sided polygonal cavity with arbitrary shape parameters, which is then applied to investigate different types of irregular hexagonal microcavities, with a focus on the formation and tuning of hexagonal WGMs in an analytical way that covers all possible shape parameters. We further explore the effect of the irregularity on the loss mechanism, including the pseudointegral loss and directional emission, which are closely related to the shape dependence of the cavity Q-factor. The conclusions drawn by the analytical equations of geometry are confirmed by the results of numerical simulations using the finite difference time domain (FDTD) method. Our fully deterministic analytical approach is necessary for obtaining better general knowledge of irregular polygonal microcavities, which would be significant for extending the scope of the understanding of WGMs, and it would provide a practical analyzing tool for experimentalists working on irregular-shaped polygonal microcavities.

We start from the most general model of an N-sided polygon shown in Fig. 1(a), where an N-WGM makes a trajectory of a closed loop of an N-sided polygon. Following the loop,
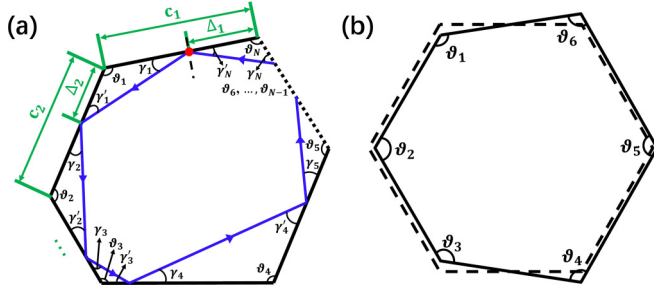
*felix831204@xjtu.edu.cn

FIG. 1. Schematic geometry of an N-sided polygon and a bent hexagon. (a) An N-sided polygon denoted by black lines. The blue solid line represents the trajectory of light (ray) incident from the red point and propagates in a counterclockwise direction. c_i is the length of the ith side of the cavity. Δ_i is the distance between the reflection point of the ray at the ith side and one end of the ith side. We take the side from which the ray enters the cavity as $i = 1$. (b) A bent hexagon (black solid lines) and its corresponding regular one (black dashed lines).

a light ray starting at a certain point [red spot in Fig. 1(a)] with an initial angle γ_1 between the side and the ray (which is complementary to the reflection angle, and is referred to as "ray angle" hereafter) should return to the same point after reflecting at each side of the polygon, while the reflection law of light requires equal reflection angles (and thereby their complementary angles) at each side of the polygon. Geometry thereby gives the following relations:

$$\gamma_{i+1} = \gamma_i' = \pi - \vartheta_i - \gamma_i, \tag{1a}$$

$$\gamma_1 = \gamma_N' = \pi - \vartheta_N - \gamma_N, \tag{1b}$$

where $i = 1, 2, 3, \ldots, N$. The ith internal angle is ϑ_i, and γ_i (γ_i') is the reflecting (incident) ray angle between the ray trajectory and the ith [$(i + 1)$th] side of the polygon, counting from the ray starting point as shown in Fig. 1(a). Applying Eq. (1a) on all sides of the polygon yields

$$\gamma_N = \pi - \gamma_1 - \sum_{i=1}^{N-1} (-1)^{i-1} \vartheta_i, \quad N \text{ is even}, \tag{2a}$$

$$\gamma_N = \gamma_1 + \sum_{i=1}^{N-1} (-1)^{i-1} \vartheta_i, \quad N \text{ is odd}. \tag{2b}$$

Applying the boundary condition Eq. (1b) yields

$$\sum_{i=1}^{N} (-1)^{i-1} \vartheta_i = 0, \quad N \text{ is even}, \tag{3a}$$

$$\pi - \sum_{i=1}^{N} (-1)^{i-1} \vartheta_i = 2\gamma_1, \quad N \text{ is odd}. \tag{3b}$$

If we temporarily ignore the requirement of TIR at every side of the polygon, Eq. (3a) reveals that polygonal cavities with an even number of sides show a strong constraint for the possibility to support N-WGMs: the sums of odd-numbered and even-numbered internal angles of the polygon must be equal. Therefore, one can easily judge whether it is possible for a hexagonal cavity to support 6-WGMs without any specific analysis by such a criterion. For example, in the

bent hexagonal cavity [41] that exhibits two slightly slanted sides due to material strain [shown in Fig. 1(b)], ϑ_1, ϑ_3, and ϑ_5 increase while ϑ_2, ϑ_4, and ϑ_6 decrease compared to the regular hexagon, which clearly does not satisfy the criterion of Eq. (3a). Therefore, none of the hexagonal cavities bent in this way support 6-WGMs, regardless of the details of the bent angle and side lengths. Such a conclusion is thoroughly deterministic compared to the ray-tracing method using a Poincaré surface of section (PSOS) [22] or optical wave simulation, which has to be applied with specific shape parameters.

Nevertheless, it should be noted that Eqs. (3a) and (3b) are necessary rather than sufficient conditions to judge the existence of N-WGMs, despite its simplicity and straightforwardness. Indeed, these two equations are derived merely from the requirement of equal incident and reflection angles on each side, but this simply misses the fact that the reflecting points should be geometrically on the sides instead of on their extension lines. This additional condition requires us to take into consideration the length of each side in the geometry. In the triangle enclosed by the light ray and any two adjacent sides, the triangular relation yields

$$\Delta_{i+1} \sin \gamma_i' = (c_i - \Delta_i) \sin \gamma_i, \tag{4a}$$

$$\Delta_1 \sin \gamma_N' = (c_N - \Delta_N) \sin \gamma_N, \tag{4b}$$

where Δ_i must satisfy

$$0 < \Delta_i < c_i, \tag{5}$$

in which c_i and Δ_i are defined in Fig. 1(a). Combining the side constraint Eq. (4a) and the angle constraint Eq. (1a) while applying the boundary conditions for both, i.e., Eqs. (4b) and (1b), yields the final expressions

$$c_N \sin \left[\pi - \sum_{i=1}^{N-1} (-1)^{i-1} \vartheta_i - \gamma_1 \right]$$
$$- \sum_L c_L \sin \left[\sum_{i=1}^{L-1} (-1)^{i-1} \vartheta_i + \gamma_1 \right]$$
$$+ \sum_M c_M \sin \left[\pi - \sum_{i=1}^{M-1} (-1)^{i-1} \vartheta_i - \gamma_1 \right] = 0, \quad N \text{ is even}, \tag{6a}$$

$$c_N \sin \left[\sum_{i=1}^{N-1} (-1)^{i-1} \vartheta_i + \gamma_1 \right]$$
$$- \sum_L c_L \sin \left[\pi - \sum_{i=1}^{L-1} (-1)^{i-1} \vartheta_i - \gamma_1 \right]$$
$$+ \sum_M c_M \sin \left[\sum_{i=1}^{M-1} (-1)^{i-1} \vartheta_i + \gamma_1 \right]$$
$$- 2\Delta_1 \sin \gamma_1 = 0, \quad N \text{ is odd}, \tag{6b}$$

where $L = N-1, N-3, \ldots$; $M = N-2, N-4, \ldots$.

Using Eqs. (6a) and (6b) constrained by Eq. (5), one can deterministically analyze any irregular polygonal microcavity for its N-WGMs. This method is extremely suitable for polygons with an even number of sides, such as hexagons, by performing the following steps:

(i) By substituting the shape parameters of the cavity into Eq. (6a), we directly obtain the value of the initial ray angle γ_1 in a deterministic way.

(ii) Applying Eq. (1a) we obtain all the ray angles γ_i, and then using Eq. (4a) we obtain the position of all reflecting points Δ_i expressed as a function of Δ_1.

(iii) Finally, we substitute all Δ_i (expressed by Δ_1) into Eq. (5) to obtain N corresponding inequalities of Δ_1, the intersection of which gives the condition that Δ_1 has to meet to allow the existence of N-WGMs. In particular, there are cases in which Δ_1 unconditionally satisfies (violates) all these N inequalities, corresponding to an irregular-shaped cavity supporting N-WGMs with all (none of) the possible shape parameters.

It should be noted that in step (i), shape parameters can be given as variables instead of fixed values, indicating the ability of reaching a global conclusion about a certain type of irregularity instead of only specific cases. The advantage of this method is to allow very straightforward analysis of an irregular-shaped hexagonal cavity without going into the complicated details of geometrical calculations each time.

We now focus on several types of irregular hexagonal microcavities. In particular, if a hexagon shows shape variations only in side length while all the internal angles ϑ_i remain $2\pi/3$, Eq. (1a) reduces to

$$\gamma_i + \gamma_{i+1} = \frac{\pi}{3}, \tag{7}$$

meaning that the ray angles of 6-WGMs of such an irregularity can either be exactly $\pi/6$ or can be alternately two values, γ_1 and $\pi/3 - \gamma_1$, where γ_1 can be obtained from Eq. (6a).

The first type of irregularity in which we are interested is the "elongated hexagon," as it is called in this context, which has two parallel sides longer than the other four. As illustrated in Fig. 2(a), the lengths of the long and short sides of the elongated hexagon are denoted as a and b, respectively. After substituting all shape parameters, Eq. (6a) yields $\gamma_1 = \pi/6$, and thus one concludes all ray angles $\gamma_i = \pi/6$ from Eq. (7), which is the same for regular hexagonal cavities. We express all values of Δ_i by Δ_1 using Eq. (4a), and we obtain a group of six inequalities of Δ_1 from Eq. (5). The intersection of these six inequalities yields the conditions for 6-WGMs to exist, which can be written as

$$b < a < 2b, \tag{8a}$$
$$a - b < \Delta_1 < b. \tag{8b}$$

It is a very special geometry that the existence of 6-WGMs depends on the position of the reflection point rather than merely the shape parameters, which leads to a specific channel of leakage in addition to the pseudointegrable loss. In Fig. 2(a) we draw a hexagon satisfying Eq. (8a), in which the blue solid line and the red dashed line correspond to the hexagonal optical loops satisfying Eq. (8b), while the green dotted line portrays the light trace violating Eq. (8b), which leaks out near the corner of the hexagon at normal incidence and results in directional emission. In reality, although closed hexagonal loops can form in the regime of Eq. (8b), the optical wave can dynamically tunnel to directional leaking channels violating Eq. (8b). In particular, when the degree of elongation increases, i.e., when the value of $(a-b)$
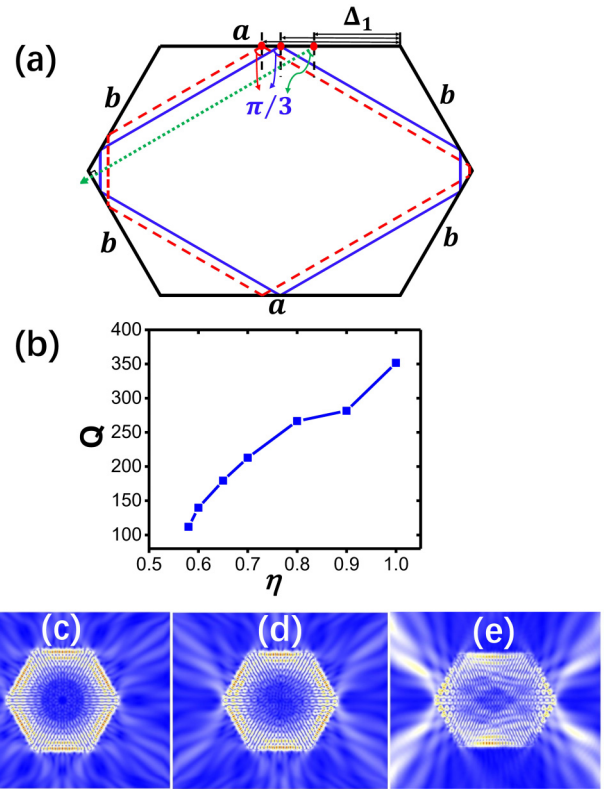

FIG. 2. Schematic geometry of an elongated hexagonal cavity and 6-WGMs in it. (a) Elongated cavity with a ratio $\eta = 0.6$ and its 6-WGMs. The blue solid line represents light incident from the middle point of the long side. The red dashed line (green dotted line) represents light incident from a nonmiddle point meeting (violating) the criterion of Eq. (8b). (b) Cavity Q-factor of the 46th mode order simulated by the FDTD of cavities with a different ratio η. Wave optics simulations of 6-WGM of the 46th mode order in elongated hexagons with (c) $\eta = 1$, (d) $\eta = 0.9$, and (e) $\eta = 0.6$.

becomes larger, the chance for $a-b < \Delta_1$ decreases, leading to greater directional leakage. This can be clearly identified from FDTD simulations as shown in Figs. 2(c)–2(e), where the directional leakage overwhelms the pseudointegrable loss with an increased degree of elongation. Therefore, the slightly elongated hexagonal cavities could serve as tunable directional emitting lasers by varying the side length ratio $\eta = b/a$. Figure 2(b) shows that the Q-factor decreases continuously with an increased degree of elongation (or a decrease of ratio η), due to the increased directional leakage. The Q-factor herein is generally low (hundreds) due to the relatively low material refractive index ($n = 1.8$) that we set for simulation, which allows us to focus on the hexagonal modes by avoiding triangular modes.

When the degree of elongation increases to violate Eq. (8a), 6-WGMs do not exist as Eq. (8b) cannot be met anymore. It should be noted that in such a regime, a different hexagonal mode with multiple reflections on the parallel long sides can survive at some specific shape parameters [36], which is nevertheless beyond the scope of our interest.

The second type of irregular shape that has been experimentally demonstrated to support WGMs is a "shortened hexagon," as it is called in this context, which has alternately long (length = a) and short (length = b) sides while keeping
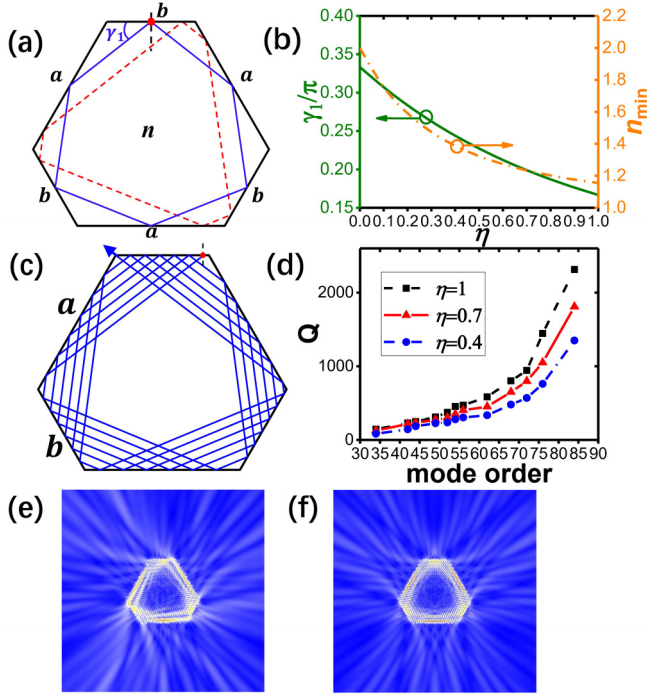
FIG. 3. Schematic geometry of a shortened hexagonal cavity and its 6-WGMs. (a) Light ray orbits of 6-WGMs. The blue solid line and the red dashed line represent orbits reflecting at the middle point and somewhere else on each side, respectively. (b) γ_1 and $n_{\min}$ as a function of η. (c) Light ray orbits with a slight deviation from the proper reflection angle. (d) Cavity Q-factor as a function of mode order for three different $\eta = 0.4$, 0.7, and 1. Field distribution of (e) traveling and (f) standing WGMs of the 51th order. The simulated cavity exhibits $\eta = 0.6$ and $n = 1.8$.

equal internal angles (i.e., $2\pi/3$), as illustrated in Fig. 3(a). Contrary to the situation of an elongated hexagon, the shortened hexagon shows very different details of light trajectory. By substituting all shape parameters into Eq. (6a) [herein we suppose that the beam starts from one of the short sides, as shown in Fig. 3(a)], we obtain

$$\frac{\sin(\gamma_{2j})}{\sin(\gamma_{2j-1})} = \frac{\sin(\gamma'_1)}{\sin(\gamma_1)} = \frac{b}{a} = \eta, \tag{9a}$$

$$\gamma_{2j-1} + \gamma_{2j} = \frac{\pi}{3}, \tag{9b}$$

where $j = 1, 2, 3$, with Eq. (7) taken into consideration, indicating that there are two alternate values of ray angles (thereby reflection angles) corresponding to the reflection point on the short and long sides, respectively, determined by η, which is a different characteristic from regular and elongated hexagons whose reflection angles are all fixed at $\pi/3$. The group of six inequalities of Δ_1 obtained from Eqs. (4a) and (5) are all naturally satisfied provided $0 < \Delta_1 < b$, meaning the existence of 6-WGMs regardless of shape parameters. As shown in Fig. 3(a), a shift of the reflection point positions on the sides (red dashed line versus blue solid line) does not break the closed hexagonal orbits, in sharp contrast to an elongated hexagon. According to Eq. (9a), the relation between η and γ_1 is plotted in Fig. 3(b), and a clear monotonous trend can be recognized. In particular, the ray angle $\gamma_1 = \pi/6$ [or $\gamma_1/\pi = 1/6$; see Fig. 3(b)] when $\eta = 1$, meaning that the model

reduces to a regular hexagon. On the other hand, the maximum of γ_1 approaches $\pi/3$ [or $\gamma_1/\pi = 1/3$; see Fig. 3(b)] when η reduces to zero, where the hexagon becomes a triangle whereas 6-WGMs no longer exist. TIR requires the material refractive index n to satisfy $n > 1/\sin(\pi/2 - \gamma_1)$ (supposing the hexagonal structure is surrounded by air), and the required minimum refractive index $n_{\min}$ is plotted as a function of η in Fig. 3(b). It is clearly shown that for all possible values of η, the value of $n_{\min}$ is always less than 2, which is the $n_{\min}$ required by 3-WGMs and D3-WGMs. Although the shortened hexagon needs to work at a higher refractive index than the regular one, its 6-WGMs still win the triangular WGMs in terms of the $n_{\min}$ requirement, therefore photonic devices can be well constructed with materials having a refractive index less than 2 by choosing the corresponding η.

Such a shortened hexagonal cavity bridges the regular hexagonal ($\eta = 1$) and regular triangular ($\eta = 0$) cavities. Though different in the characteristic of reflection angles, the shortened hexagon shows the same mechanism of pseudointegrable loss as the regular one [42]. As illustrated in Fig. 3(c), a tiny deviation from the proper reflection angle of $\pi/2 - \gamma_1$ leads to a successive shift of the reflection point on the short side during each round trip of the light ray, which eventually leaks out when the reflection point shifts to the corner. In a cavity with a given circumference, $C = 3(a + b)$, a smaller value of b increases the pseudointegrable loss as a light ray with a certain deviation from the proper reflection angle takes a shorter circulation time to come to the corner and leak out. This is verified by the Q-factor, which decreases with the reduction of η, as shown in Fig. 3(d). The leakage mechanism is further revealed by field distribution analysis, as shown in Figs. 3(e) and 3(f). The traveling WGM exhibits major emission from the corners of the hexagon [Fig. 3(e)], while the standing WGM can be viewed as a linear superposition of two counterpropagating traveling WGMs [Fig. 3(f)]. We note that the total leakage is also dependent on the ratio between the cavity size and the optical wavelength C/λ, which determines the mode order. With increasing (decreasing) mode order, the confined light is more raylike (wavelike), giving rise to less (more) uncertainty of the reflection angle and thereby leading to smaller (larger) pseudointegrable loss, as seen in Fig. 3(d).

Finally, we discuss the irregularity that Song *et al.* [43] have conceived as an intermediate shape for the theoretical demonstration of the strong coupling of triangular superscar modes in regular hexagons, although still with neither experimental demonstration nor theoretical studies of 6-WGMs. The proposed cavity, called a "shifted cavity" in this context, is illustrated in Fig. 4(a). The cavity is constructed by simply shifting the topmost side of a regular hexagon [black solid line in Fig. 4(a) with side length a] either upward or downward [red dashed line in Fig. 4(a)] by a distance δ, leading to unchanged internal angles and three different values of side lengths: a, $a - 2\delta/\sqrt{3}$, and $a + 2\delta/\sqrt{3}$, as shown in Figs. 4(b) and 4(c). Similar to the two types of cavities discussed above, a deterministic analysis performed by Eqs. (4a)–(6b) yields the conditions for supporting 6-WGMs in the case of the upshifted topmost side,

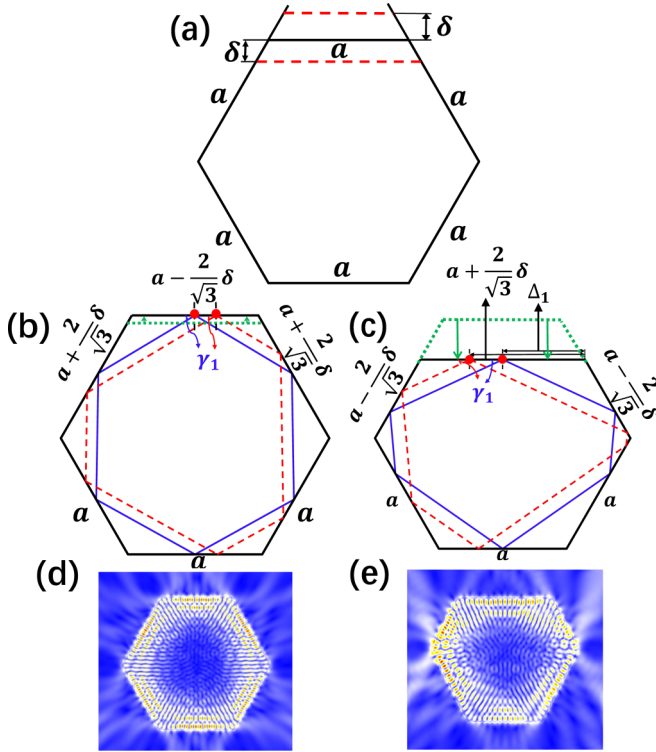$$\tan(\gamma_1) = \frac{\sqrt{3}}{3} + \frac{4\delta}{9a}, \tag{10}$$

FIG. 4. Image of 6-WGMs in a shifted hexagon. (a) Schematic geometry of a shifted hexagon with the upshifted and downshifted topmost side represented by a red dashed line. The blue solid line and the red dashed line in (b) the upshifted hexagon and (c) the downshifted hexagon represent light incident from the midpoint and somewhere else on the side. Green arrows denote the movement of the upshifted and downshifted topmost side in (b) and (c), respectively. Parts (d) and (e) are wave optics simulation figures of an upshifted hexagon with $\delta = 0.1\,\mu$m and a downshifted hexagon with $\delta = 0.5\,\mu$m, respectively. The material refractive index is $n = 1.8$, side lengths a are equal to $2\,\mu$m, and optical modes are of the 47th order in (d) and (e).

and in the case of the downshifted topmost side,

$$0 < \frac{\delta}{a} < \frac{3\sqrt{3}}{10}, \tag{11a}$$

$$\tan(\gamma_1) = \frac{\sqrt{3}}{3} - \frac{4\delta}{9a}, \tag{11b}$$

$$\frac{3\sqrt{3}a + 2\delta}{3\sqrt{3}a - 4\delta}\left(a - \frac{2}{\sqrt{3}}\delta\right) - a\left(2 - \frac{3\sqrt{3}a + 2\delta}{3\sqrt{3}a - 4\delta}\right)$$
$$< \Delta_1 < \frac{3\sqrt{3}a + 2\delta}{3\sqrt{3}a - 4\delta}\left(a - \frac{2}{\sqrt{3}}\delta\right). \tag{11c}$$

Equation (10) indicates that the upshifted hexagon supports 6-WGMs regardless of shape parameters, similar to the shortened hexagonal cavity, while the downshifted hexagon has a constraint on the shape parameters by Eqs. (11a) and (11c), similar to the elongated hexagon. Considering Eq. (7), the values of the reflection angles are the same for the upshifted and downshifted cases. Nevertheless, they show dramatic differences in the leakage of the modes. The upshifted hexagon unconditionally supports 6-WGMs, while the downshifted hexagon, fulfilling Eq. (11a), is conditional regarding the reflection point position Δ_1 on the long side, expressed by Eq. (11c), which yields directional emission like the elongated hexagonal cavity. The FDTD simulation in Figs. 4(d) and 4(e) clearly demonstrates this difference.

Finally, the limitations of geometrical optics should be noticed, especially for discussing the loss mechanism. Although 6-WGMs are permitted in the shortened and upshifted hexagonal cavity regardless of the position of the reflection point, the pseudointegrable and boundary wave loss become very significant when the lengths of the short sides reduce to a certain extent, therefore in reality well-confined 6-WGMs cannot cover the whole range of the allowed shape parameters by geometrical optics. Unlike regular polygonal cavities, whose overall size versus optical wavelength determines the optical loss, the short sides of the investigated irregular cavities matter.

In conclusion, we developed a general method of deterministic analysis for WGMs of polygonal microcavities with irregular shapes, which provides an easy and straightforward mathematical tool for a large group of experimentalists working on such microcavities. The method is tested in various types of irregular hexagons, allowing fast determinations of the existence of 6-WGMs and predicting the particular features of each type, which agree well with the wave optics simulations and the previously reported experimental results. The proposed idea of deterministic analysis is not constrained to N-WGMs, but it can also be applied to obtain corresponding analytical equations for other types of modes (e.g., triangular WGMs in a hexagon) in any type of irregular polygonal microcavity. With the fact that theoretical conclusions have been drawn mainly on regular polygonal cavities in the past, it is essential to realize that polygonal cavities with reduced symmetry can also be described by "regular" equations and investigated in a systematic way beyond specific shape parameters.

[1] T. Harayama and S. Shinohara, Two-dimensional microcavity lasers, Laser Photon. Rev. **5**, 247 (2011).

[2] T. J. Kippenberg, R. Holzwarth, and S. A. Diddams, Microresonator-based optical frequency combs, Science **332**, 555 (2011).

[3] X.-F. Jiang, Y.-F. Xiao, Q.-F. Yang, L. Shao, W. R. Clements, and Q. Gong, Free-space coupled, ultralow-threshold Raman lasing from a silica microcavity, Appl. Phys. Lett. **103**, 101102 (2013).

[4] Q. Li, T. C. Briles, D. A. Westly, T. E. Drake, J. R. Stone, B. R. Ilic, S. A. Diddams, S. B. Papp, and K. Srinivasan, Stably accessing octave-spanning microresonator frequency combs in the soliton regime, Optica **4**, 193 (2017).

[5] L. Stern *et al.*, Direct Kerr frequency comb atomic spectroscopy and stabilization, Sci. Adv. **6**, eaax6230 (2020).

[6] S. B. Papp, P. Del'Haye, and S. A. Diddams, Mechanical Control of a Microrod-Resonator Optical Frequency Comb, Phys. Rev. X **3**, 031003 (2013).

[7] J. Li, H. Lee, T. Chen, and K. J. Vahala, Low-Pump-Power, Low-Phase-Noise, and Microwave to Millimeter-Wave Repetition Rate Operation in Microcombs, Phys. Rev. Lett. **109**, 233901 (2012).

[8] L. He, Ş. K. Özdemir, and L. Yang, Whispering gallery microcavity lasers, Laser Photon. Rev. **7**, 60 (2013).

[9] M. Schermer, S. Bittner, G. Singh, C. Ulysse, M. Lebental, and J. Wiersig, Unidirectional light emission from low-index polymer microlasers, Appl. Phys. Lett. **106**, 101107 (2015).

[10] P. Miao, Z. Zhang, J. Sun, W. Walasik, S. Longhi, N. M. Litchinitser, and L. Feng, Orbital angular momentum microlaser, Science **353**, 464 (2016).

[11] W. Chen, Ş. K. Özdemir, G. Zhao, J. Wiersig, and L. Yang, Exceptional points enhance sensing in an optical microcavity, Nature (London) **548**, 192 (2017).

[12] B. Peng, Ş. K. Özdemir, F. Lei, F. Monifi, M. Gianfreda, G. L. Long, S. Fan, F. Nori, C. M. Bender, and L. Yang, Parity–time-symmetric whispering-gallery microcavities, Nat. Phys. **10**, 394 (2014).

[13] J. Wiersig, Enhancing the Sensitivity of Frequency and Energy Splitting Detection by Using Exceptional Points: Application to Microcavity Sensors for Single-Particle Detection, Phys. Rev. Lett. **112**, 203901 (2014).

[14] R. Sarma, L. Ge, J. Wiersig, and H. Cao, Rotating Optical Microcavities with Broken Chiral Symmetry, Phys. Rev. Lett. **114**, 053903 (2015).

[15] X. Jiang, A. J. Qavi, S. H. Huang, and L. Yang, Whispering-gallery sensors, Matter **3**, 371 (2020).

[16] J. Wen, X. Jiang, L. Jiang, and M. Xiao, Parity-time symmetry in optical microcavity systems, J. Phys. B **51**, 222001 (2018).

[17] L.-K. Chen, Y.-Z. Gu, Q.-T. Cao, Q. Gong, J. Wiersig, and Y.-F. Xiao, Regular-Orbit-Engineered Chaotic Photon Transport in Mixed Phase Space, Phys. Rev. Lett. **123**, 173903 (2019).

[18] Q. Song, L. Ge, B. Redding, and H. Cao, Channeling Chaotic Rays into Waveguides for Efficient Collection of Microcavity Emission, Phys. Rev. Lett. **108**, 243902 (2012).

[19] J. Lin, Y. Huang, Y. Yang, Q. Yao, X. Lv, J. Xiao, and Y. Du, Single transverse whispering-gallery mode AlGaInAs/InP hexagonal resonator microlasers, IEEE Photon. J. **3**, 756 (2011).

[20] Y.-D. Yang, M. Tang, F.-L. Wang, Z.-X. Xiao, J.-L. Xiao, and Y.-Z. Huang, Whispering-gallery mode hexagonal micro-/nanocavity lasers, Photon. Res. **7**, 594 (2019).

[21] D. J. Gargas, M. C. Moore, A. Ni, S.-W. Chang, Z. Zhang, S.-L. Chuang, and P. Yang, Whispering gallery mode lasing from zinc oxide hexagonal nanodisks, ACS Nano **4**, 3270 (2010).

[22] H. Cao and J. Wiersig, Dielectric microcavities: Model systems for wave chaos and non-Hermitian physics, Rev. Mod. Phys. **87**, 61 (2015).

[23] Q. Zhang, S. T. Ha, X. Liu, T. C. Sum, and Q. Xiong, Room-temperature near-infrared high-Q perovskite whispering-gallery planar nanolasers, Nano Lett. **14**, 5995 (2014).

[24] A. Feng, X. Jiang, X. Zhang, X. Zheng, W. Zheng, O. F. Mohammed, Z. Chen, and O. M. Bakr, Shape control of metal halide perovskite single crystals: From bulk to nanoscale, Chem. Mater. **32**, 7602 (2020).

[25] S. T. Ha, X. Liu, Q. Zhang, D. Giovanni, T. C. Sum, and Q. Xiong, Synthesis of organic–inorganic lead halide perovskite nanoplatelets: Towards high-performance perovskite solar cells and optoelectronic devices, Adv. Opt. Mater. **2**, 838 (2014).

[26] X. Liu *et al.*, Periodic organic–inorganic halide perovskite microplatelet arrays on silicon substrates for room-temperature lasing, Adv. Sci. **3**, 1600137 (2016).

[27] L. Niu *et al.*, Controlled growth and reliable thickness-dependent properties of organic–inorganic perovskite platelet crystal, Adv. Funct. Mater. **26**, 5263 (2016).

[28] Y. Sun *et al.*, Band structure engineering of interfacial semiconductors based on atomically thin lead iodide crystals, Adv. Mater. **31**, 1806562 (2019).

[29] T. Kouno, M. Sakai, K. Kishino, and K. Hara, Excitation area dependence of lasing modes in thin hexagonal GaN microdisks, Jpn. J. Appl. Phys. **55**, 01AC03 (2015).

[30] T. Kouno, M. Sakai, K. Kishino, and K. Hara, Quasi-whispering gallery mode lasing action in an asymmetric hexagonal GaN microdisk, Jpn. J. Appl. Phys. **52**, 08JG03 (2013).

[31] H. Dong, Y. Liu, S. Sun, Z. Chen, and L. Zhang, Optical modulation in microsized optical resonators with irregular hexagonal cross-section, J. Mater. Chem. C **2**, 8976 (2014).

[32] Y. Xiong, W. Yi, G. Yang, and Y. Yang, Elongated hexagonal ZnO micro-fence optical resonator, Curr. Appl. Phys. **19**, 984 (2019).

[33] C. Dietrich, M. Lange, C. Sturm, R. Schmidt-Grund, and M. Grundmann, One- and two-dimensional cavity modes in ZnO microwires, New J. Phys. **13**, 103021 (2011).

[34] C. Dietrich, M. Lange, F. Klüpfel, H. von Wenckstern, R. Schmidt-Grund, and M. Grundmann, Strain distribution in bent ZnO microwires, Appl. Phys. Lett. **98**, 031105 (2011).

[35] Y. Zhu, Y. Zhou, M. I. B. Utama, M. de la Mata, Y. Zhao, Q. Zhang, B. Peng, C. Magen, J. Arbiol, and Q. Xiong, Solution phase van der Waals epitaxy of ZnO wire arrays, Nanoscale **5**, 7242 (2013).

[36] H. Dong, Y. Liu, S. Sun, J. Li, J. Zhan, Z. Chen, and L. Zhang, Geometry dependent evolution of the resonant mode in ZnO elongated hexagonal microcavity, Sci. Rep. **6**, 19273 (2016).

[37] H. Dong, C. Zhang, Y. Liu, Y. Yan, F. Hu, and Y. S. Zhao, Organic microcrystal vibronic lasers with full-spectrum tunable output beyond the Franck-Condon principle, Angew. Chem. **130**, 3162 (2018).

[38] Z. Yu *et al.*, Self-assembled microdisk lasers of perylenediimides, J. Am. Chem. Soc. **137**, 15105 (2015).

[39] X. Wang, Q. Liao, Q. Kong, Y. Zhang, Z. Xu, X. Lu, and H. Fu, Whispering-gallery-mode microlaser based on self-assembled organic single-crystalline hexagonal microdisks, Angew. Chem. **126**, 5973 (2014).

[40] F. Lu, I. Bhattacharya, H. Sun, T.-T. D. Tran, K. W. Ng, G. N. Malheiros-Silveira, and C. Chang-Hasnain, Nanopillar quantum well lasers directly grown on silicon and emitting at silicon-transparent wavelengths, Optica **4**, 717 (2017).

[41] M. Grundmann and C. P. Dietrich, Whispering gallery modes in deformed hexagonal resonators, Phys. Status Solidi B **249**, 871 (2012).

[42] J. Wiersig, Hexagonal dielectric resonators and microcrystal lasers, Phys. Rev. A **67**, 023807 (2003).

[43] Q. Song, L. Ge, J. Wiersig, and H. Cao, Formation of long-lived resonances in hexagonal cavities by strong coupling of superscar modes, Phys. Rev. A **88**, 023834 (2013).